Nanoscale

Experimental Determination of Single Molecule Toroic Behaviour in a Dy_8 Single-Molecule Magnet

Journal Name

ARTICLE TYPE

Experimental Determination of Single Molecule Toroic Behaviour in a Dy$_8$ Single Molecule Magnet

Qing Zhang,[a,b] Michael L. Baker,[*,c,d] Shiqi Li,[a,b] Myriam P. Sarachik,[*,a,b] José J. Baldoví,[e] Alejandro Gaita-Ariño,[f] Eugenio Coronado[f], Dimitris I. Alexandropoulos[g] and Theocharis Stamatatos.[g,h]

The enhancement of toroic motifs through coupling toroidal moments within molecular nanomagnets is a new, interesting and relevant approach for both fundamental research and potential quantum computation applications. We investigate a Dy$_8$ molecular cluster and discover it has a antiferrotoroic ground state with slow magnetic relaxation. The experimental characterization of the magnetic anisotropy axes of each magnetic center and their exchange interactions represents a considerable challenge due to the non-magnetic nature of the toroidal motif. To overcome this and obtain access to the low energy states of Dy$_8$ we establish a multi-orientation single-crystal micro Hall sensor magnetometry approach. Using an effective Hamiltonian model we then unpick the microscopic spin structure of Dy$_8$, leading to a canted antiferrotoroidic tetramer molecular ground state. These findings are supported with electrostatic calculations that independently confirm the experimentally determined magnetic anisotropy axes for each Dy^{III} ion within the molecule.

Introduction

Recent breakthroughs in the synthesis of Dy^{III} single ion magnets sees molecular based magnetic remanence reaching liquid nitrogen temperatures[1,2]. These advances make molecular nanomagnets strong contenders for magnetic data storage and molecular spintronic applications. However the dipolar fields generated by arrays of single ion magnets destabilise the bistability of magnetisation[3,4]. Consequently, the achievement of a blocking temperature of ~80 K requires the doping of Dy^{III} sites into a diamagnetic host lattice. Exchange coupling Dy^{III} ions opens up additional degrees of freedom for the organisation of quantum states. One interesting outcome from studying polynuclear Dy^{III} clusters has been the identifcation of ground states with novel non-collinear spin configurations.[5–12] Molecular based toroidal

magnetism in Dy^{III} coordination clusters have the advantages of generating much weaker dipolar fields while also being insensitive to stray magnetic fields making the possibility of higher information storage densities than single ion magnets. Furthermore, single molecule toroics (SMTs) are shown to have a sensitivity to magneto-electric coupling[13] resulting in magnetoelectric and magnetocurrent properties[14,15] desirable for molecular spintronic applications. Regardless of opinions concerning future applications, the development of an increasingly diverse range of polynuclear clusters gives rise to a rich test-bed of prototype molecules to study the fundamental aspects of SMTs.

First indications of SMT properties were proposed following the identification of a close to non-magnetic ground state in a triangular Dy$_3$ molecule.[5,16,17] *Ab initio* calculations identified each Dy^{III} ion as having a large axial magnetic anisotropy, with local magnetic easy axes that form a nearly toroidal arrangement within the plane of the Dy$_3$ triangle[18]. Since the initial studies on Dy$_3$, it is now recognised that the toroidal motif manifests in an increasing range of more complex clusters including lower symmetry triangles[9], multiple triangular units[8,10–12], larger cyclic arrangements[6,7] and cubanes[19]. The arrangement of the Dy^{III} ions in combination with molecular symmetry affords SMT ground states with various combinations of toroidal moment and magnetisation. For instance, high symmetry cyclic clusters such as Dy$_4$[6] and Dy$_6$[7] exhibit a toroidal non-magnetic singlet ground state, while the single ion magnetisation in lower

[a] Department of Physics, Graduate Center, CUNY, New York, New York 10016, USA
[b] Department of Physics, City College of New York, CUNY, New York, New York 10031, USA; E-mail: msarachik@ccny.cuny.edu
[c] The School of Chemistry, The University of Manchester, M13 9PL Manchester, United Kingdom; E-mail: michael.baker@manchester.ac.uk
[d] The University of Manchester at Harwell, Didcot, OX11 0FA, UK.
[e] Max Planck Institute for the Structure and Dynamics of Matter, Luruper Chaussee 149, 22761 Hamburg, Germany.
[f] Instituto de Ciencia Molecular (ICMol), Universitat de València, C/Catedrático José Beltrán, 2, E-46980 Paterna, Spain
[g] Department of Chemistry, Brock University, L2S 3A1 St. Catharines, Ontario, Canada
[h] Present address: Chemistry Department, University of Patras, Patras 26504, Greece

symmetry clusters, including Dy$_3$, does not fully cancel, leading to weakly magnetic ground states in combination with toroidicity.[9] Examples of molecules composed of multiple triangular units exist for both cases where individual toroidal moments are enhanced and cases where the toroidal moments oppose.[6–8,10,11,20] In all of these cases toroidal texture of states has been identified by theoretical calculations. Calculations based on the coordination geometry has proven indispensable for the identification and classification of SMTs. It is equally important to find experimental evidence for SMTs to support theoretical characterisation. A vanishing, or close to vanishing, molecular magnetic moment in the ground state is a distinctive characteristic of SMTs, which makes experimental identification of ground state easy axis orientations a considerable challenge. Muon spin relaxation measurements have been shown successful in probing the static local field generated by Dy ions within Dy$_3$ ground state[21]. The most rigorous published experimental studies performed to date have been by van Slageren *et al.*[22] where a variety of methods were applied to investigate the original Dy$_3$ compound. The conclusion of that study was that a combination of experimental techniques was required, with far-infrared spectroscopy and out-of-plane torque magnetometry measurements being the most insightful. However the most appropriate choice of experimental method depends on the specific molecular symmetry of the compound under study. In the case of Dy$_3$ experimental determination of Dy site easy axis orientations using single-crystal magnetisation measurements is restricted since the cluster symmetry closely follows the symmetry of the triangular toroidal unit. In this study we identify that this restriction is lifted when the molecular rotational symmetry axis is not collinear with the individual toroidal axes. It is demonstrated that multiple orientation magnetisation measurements can be used to derive the single ion easy axis orientations within a SMT.

For this study, we selected the octanuclear compound (Et$_4$N)$_4$[Dy$_8$O(nd)$_8$(NO$_3$)$_{10}$(H$_2$O)$_2$], (here after, Dy$_8$; nd^{2-} is the dianion of naphthalene-2,3-diol) which is a structural analogue of the recently reported family of Ln$_8$ clusters[23]. The Dy$_8$ analogue was fully characterized by powder XRD, IR and elemental analysis studies as well as unit cell comparison with authentic single-crystals of the crystalllographically determined Tb$_8$ analogue[23]. Earlier measurements provided potential evidence for weak antiferromagnetic coupling and alternating current susceptibility measurements show frequency dependence in the out-of-phase susceptibility below 9 K.[23] The structure of the Dy$_8$ anion is shown in Fig. 1(a), and it possesses crystallographic C_1 symmetry. From a chemical perspective the core of Dy ions and their bridging ligands have a virtual S_4 symmetry. This central unit consists of the [Dy$_4(\mu_4$-O^{2-})] tetrahedron whose four edges are each fused with the edge of a Dy$_3$ triangle (supporting Fig. S1). The resulting Dy$_8$ core (Fig. 1(b)) has a structurally and magnetically unique topology, which is reminiscent of a distorted snub-square, Archimedean tiling unit. The central Dy$_4$ tetrahedron pitches the individual Dy$_3$ triangles out of the mean (X-Y) plane of the molecule (Fig. 1(b) and (c)). The rotational symmetry of the molecule differs from that of the individual triangular units, an aspect that we found is important for applying multi-
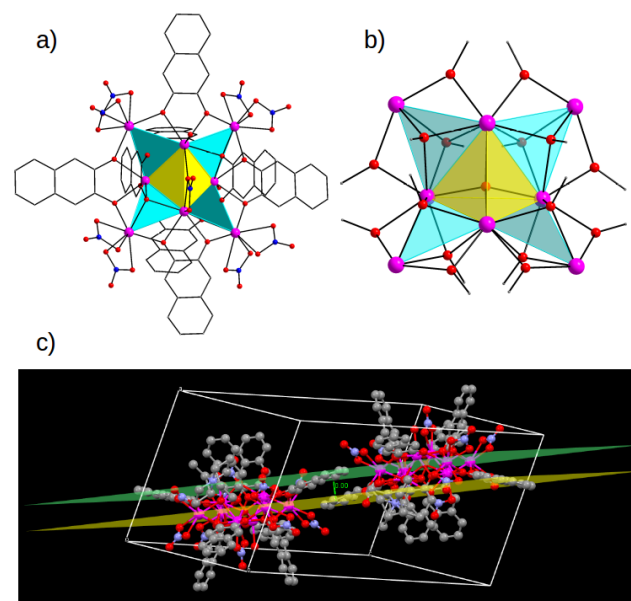

Fig. 1 (a) The structure of the [Dy$_8$O(nd)$_8$(NO$_3$)$_{10}$(H$_2$O)$_2$]$^{4-}$ cluster anion, where nd^{2-} is the naphthalene-2,3-dialkoxide dianion. (b) The [Dy$_8$O(OR)$_{16}$]$^{6+}$ core, where μ_4-O^{2-} is at the center of the Dy$_4$ tetrahedron and the μ_2/μ_3-OR groups belong to the alkoxide arms of naphthalene-2,3-dialkoxide, serving to link the four external Dy$_3$ triangles with the Dy$_4$ tetrahedron. (c) Packing diagram showing the orientation of the best-mean-planes between adjacent octanuclear clusters in the crystal. Colour code: Dy^{III} purple, O red, N blue, C gray and H excluded for clarity.

ple orientation magnetisation as a means to determine easy axis orientations. According to the X-ray structure of the Tb$_8$ analogue, the octanuclear clusters pack in a parallel but opposite fashion (angle between best-mean-planes of adjacent molecules is 0°, 1(c)), while the voids between the cluster anions are occupied by Et$_4$N$^+$ countercations and lattice solvate molecules. The octanuclear clusters are also well-separated from each other in the crystal; for the Tb$_8$ analogue, the shortest Tb-Tb intermolecular distance is $\sim$ 9 Å.

Results

Magnetic Properties

Magnetic susceptibility measurements on a polycrystalline sample of Dy$_8$ show that the χT product remains constant as the temperature is lowered from 300 to 100 K and then decreases as the temperature is further reduced, indicating thermal depopulation of Dy^{III} ion crystal field excited states (see supporting information). The magnetic susceptibility measured at 0.1 T (green triangles, Fig. 2) rises to a peak at 5 K, and decreases sharply on further cooling, indicating weak antiferromagnetic exchange interactions between Dy^{III} ions within Dy$_8$ molecules. Single-crystal susceptibility measurements identifies a easy X-Y plane within the plane of the crystal and a hard Z-axis perpendicular to the plane of the crystal. The magnetic easy X-Y plane aligns with the best mean-plane of Dy$_8$. With a 0.1 T field applied within the X-Y plane of Dy$_8$, the susceptibility follows a similar trend with respect to the powder measurements, rising to a maximum 2 cm^3
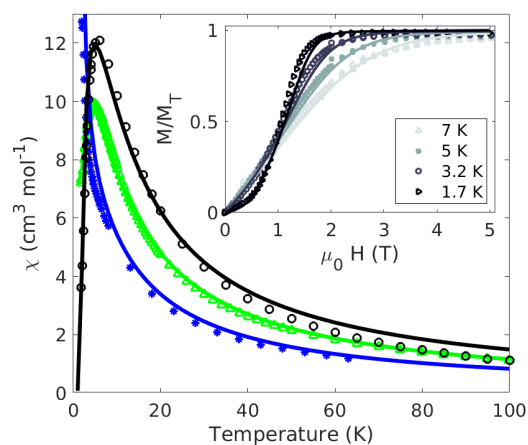
Fig. 2 The temperature-dependence of magnetic susceptibility for Dy_8 with an applied field of 0.1 T for an orientation averaged (green open triangles), and a single-crystal sample with the field aligned within the molecular X-Y plane (black circles) and along the hard Z axis (blue stars), with calculations (solid lines). Insert: Single-crystal magnetisation measurements of Dy_8 with the field applied within the X-Y plane measured at 1.7 K, 3.2 K, 5 K and 7 K, symbols represent the data and simulations are shown as solid lines.

mol^{-1} greater than the powder at 5 K (black circles, Fig. 2). From the 5 K to 1.8 K the susceptibility decreases more severely than the powder measurement towards zero, providing further evidence for an antiferromagnetic ground state. With the applied field perpendicular to the plane of the molecule the susceptibility increases on decreasing temperature (blue stars, Fig. 2). This behaviour differs with respect to single-crystal studies on isolated Dy_3 triangles where the hard axis susceptibility is close to temperature independent. The out-of-plane magnetisation indicates that single ion Dy^{III} magnetisation axes have substantial components projecting out of the X-Y plane of the molecule.

Low temperature single-crystal measurements with fields applied within the X-Y plane reveal a strong inflection (or S-shape) from 0 to 2 T indicating a non-magnetic ground state, with the magnetisation saturating (M_T) above 2 T, Fig. 2 inset. To investigate the magnetisation dynamics of Dy_8 at lower temperatures we performed measurements down to 0.25 K using a micro-Hall-bar array. Fig. 3a shows the X-Y plane magnetisation at various temperatures. The lowest temperature magnetisation measurements reveal three steps in the field dependence of magnetisation with slow magnetic relaxation that results in a hysteresis ranging from -1.9 to 1.9 T. The hysteresis is temperature and field sweep rate dependent, closing by 2 K at 20 mT/sec. The first step in magnetisation is observed on crossing zero field from both positive and negative applied field directions, indicating quantum tunnelling of magnetisation. Further steps in magnetisation are only observed on increasing field magnitude. The first applied field step (c_1) and the second applied field step (c_2) are most precisely identified as maxima in first derivative of the magnetisation (dM/dH) on increasing field magnitude (Fig. 3a lower pannel). The steps c_1 and c_2 are ground state crossings that correspond to the Zeeman energy required to flip the magnetisation of individ-
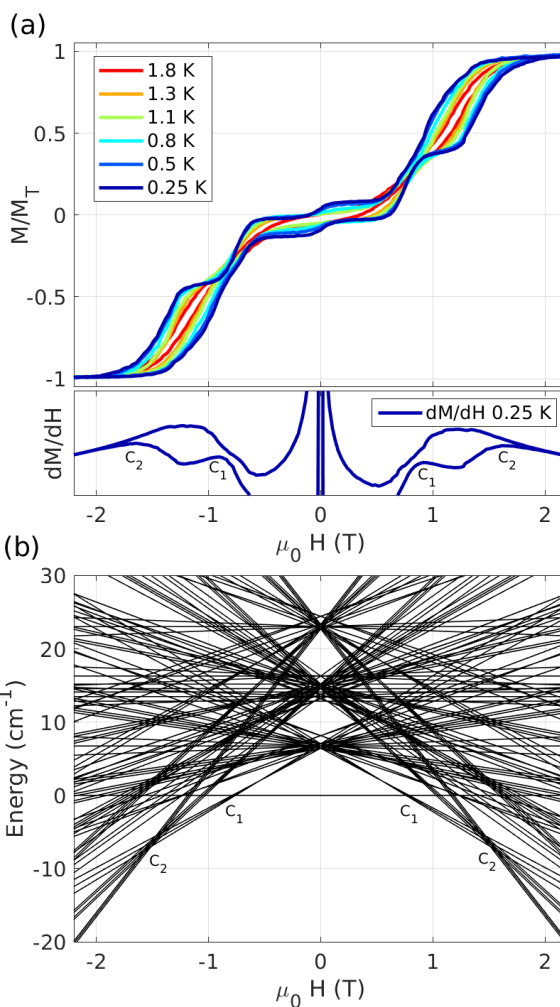

Fig. 3 (a) Applied field dependence of single-crystal Hall bar magnetisation, measured for various temperatures within the molecular X-Y plane with a magnetic field sweep rate of 20 mT/sec. At 0.25 K two clear steps in the magnetisation are observed, most clearly are identified as maxima in dM/dH (labelled c_1 and c_2), on increasing magnitude of applied field. (b) Zeeman diagram corresponding with data in (a) based on Hamiltonian (1).
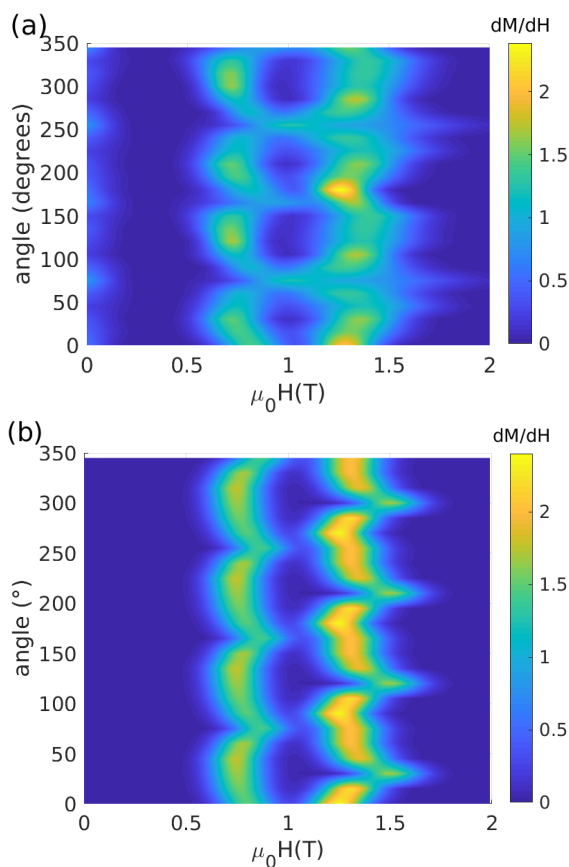
Fig. 4 Measured (a) and calculated (b) first derivative of magnetisation (dM/dH) plotted as a function of sample orientation within the molecular X-Y plane at 0.3 K. An angle of zero corresponds with the magnetic field vector at 45° from the molecular X and Y axes. Maxima in dM/dH for a given angle correspond with field crossings referred to in the text as c_1 and c_2. Calculations are based on Hamiltonian (1) described within the text.
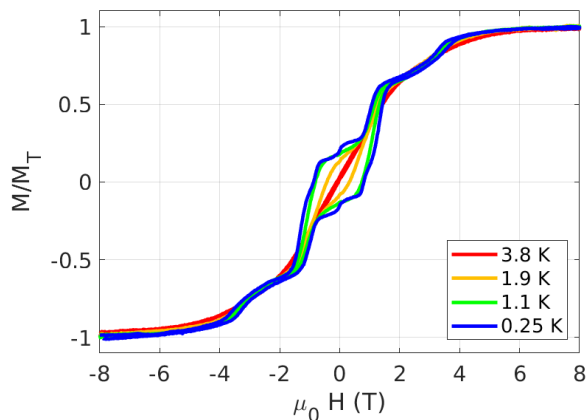

Fig. 5 Single-crystal Hall bar measurements at various temperatures with an applied field sweep rate of 20 mT/sec. (a) Measurements with the applied field along the molecular Z, hard axis.

the magnetisation increases further and approaches saturation by 8 T indicating the potential admixture of excited Stark levels, as described for Dy_3 [5].

Analysis and Characterisation

Before attempting to fit the experimental data, we test the robustness of variable crystal orientation magnetisation measurements as a method to obtain the Dy ion easy axis orientations. The full Dy ion spin-orbit coupled $J=15/2$ manifold for large Dy clusters results in prohibitively large Hamiltonian matrix dimensions (some 4.3 billion states for Dy_8). The exchange Hamiltonian matrix dimension can be vastly reduced by excluding all but the thermally populated states and including only the lowest energy Kramers doublet for each single ion. We model the single ion Kramers doublets with g-tensor principal values of $g_{zz} = 20$ and $g_{xx} = g_{yy} = 0$. The effective model is described using a $S = 1/2$ Ising Hamiltonian that couples effective doublets as follows:

$$H = -\sum_{i>k} J_{zz} S_{z_i} \cdot S_{z_k} - \mu_B \sum_{i}^{8} g_i H_z S_{z_i} \qquad (1)$$

where i,k are the nearest neighbours (illustrated as black lines in Fig. 6). The principal directions of the local anisotropy axis z_i are specific to each Dy ion. The fourfold rotational symmetry of the measured in-plane magnetisation (Fig. 4) sets boundary conditions for Dy ion easy axis orientations within each of the four Dy-triangles. The schematic in Fig. 6 shows the ϕ angles within the local triangle reference frame that define the easy axis orientations for the Dy ions. Similarly the out-of-plane angles are defined as θ_1 and θ_2 and are close to zero. Calculations were performed varying the θ and ϕ angles (see examples in the supporting information). These calculations indicate that the phase in oscillations of c_1 and c_2 depend strongly on ϕ_1 and ϕ_2. The amplitude of the oscillations in c_1 and c_2 is found to depend on θ_1 and θ_2. To fit the measured magnetic field and temperature dependence of the magnetisation for Dy_8 requires adjustment of both exchange interactions (J_{zz}) and the principal anisotropy axis for the eight

ual Dy ions within Dy_8. The Zeeman diagram, Fig. 3b, shows the crossings at fields corresponding with c_1 and c_2. The precise applied magnetic field values of c_1 and c_2 are found to have a dependence on the single-crystal orientation within the X-Y plane. The crossings relate to both the intra-molecular exchange interactions between Dy ions and the relative orientation of the Dy ion easy axes with respect to the direction of the applied magnetic field. Single-crystal magnetisation measurements performed in the X-Y plane of Dy_8 at 0.3 K clearly identifies orientation dependence in the field crossings c_1 and c_2 that follow a periodic fourfold orientation dependence, Fig. 4. The maximum field for c_1 is observed with the magnetic field vector aligned along the molecular X or Y axis. The higher field crossing c_2 is 90 degrees out of phase with c_1 and has a lower amplitude within its field variation. Assuming a fourfold symmetry indicates equivalence in Dy-Dy exchange interactions and the relative orientations of Dy ion easy axis within the four triangles. Hall bar magnetisation measurements with the applied magnetic field aligned along the molecular Z axis reveal a magnetic hysteresis that persists up to around 3.8 K, Fig. 5. The 0.25 K measurement includes multiple steps in its magnetisation at approximately 0, ±0.8, ±1.6, and ±3.7 T. Above 4 T
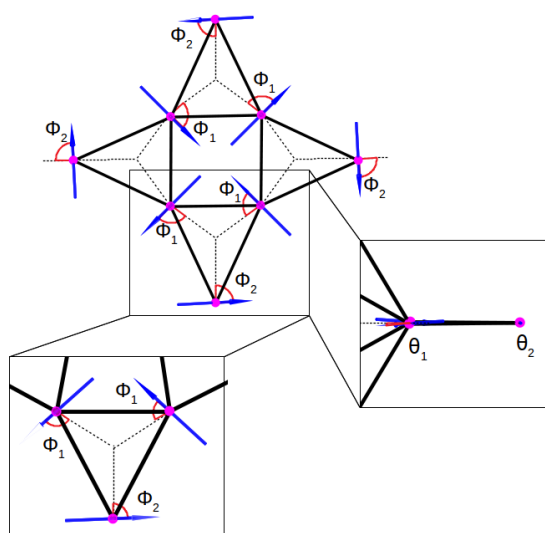
Fig. 6 A schematic of Dy ion easy axis orientations determined for Dy_8. The two inserts show the lower Dy-triangle from perspectives perpendicular to and within the plane of the triangle. The easy axis orientations are defined within the plane of the Dy-triangle. The angles $\phi_1 = 90°$ and $\phi_2 = 87°$ are defined with respect to the bisector of the triangle. The out-of-plane component to the single ion easy axes are defined perpendicular to the plane of the triangle. These angles are close to zero ($\theta_1 = 5°$ and $\theta_2 = 0°$).

Fig. 7 Schematic views of the central core of Dy ions (purple spheres). Green arrows show the canted nature of the four toroic moments within the ground state.

Dy ions (described by ϕ_1, ϕ_2, θ_1 and θ_2). The magnitude of J_{zz} controls the absolute applied magnetic field of the crossings ($c1$ and $c2$). The best fit to experimental data was determined by numerically evaluating the field dependence for the full parameter space (J_{zz}, ϕ_1, ϕ_2, θ_1 and θ_2). The fitting procedure was focused on obtaining the measured c_1 and c_2 as a function of crystal orientation. It was found that inclusion of just one nearest neighbour exchange constant is required to fit the experimental data. Fig. 4 shows the best fit to field crossing data where $J_{zz} = $ -10.92 cm^{-1}, $g_z = 20$, $\phi_1 = 90°$, $\phi_2 = 87°$, $\theta_1 = 5°$ and $\theta_2 = 0°$. The best fit parameters also compare well to higher temperature magnetisation and susceptibility measurements (Fig. 2). The exchange constant determined for Dy_8 is slightly larger in magnitude than that of Dy_3 (-7.4 cm^{-1}). The Zeeman diagram for the out of plane magnetisation shows low energy excited state level crossings at 0.62, 1.28, 1.88, 2.14 and 2.56 T and two ground state level crossings at 2.0 and 2.84 T (supporting information). The fit to the low temperature out of plane magnetisation data could perhaps be improved with the inclusion of a small amount of state mixing with excited Stark levels. However extension of our model to include such contributions is inhibited by the excessively large Hamiltonian dimension that results. Furthermore misalignment in crystal due to the crystals plate like morphology creates an uncertainty in the out of plane alignment of $\pm$ 5 degrees for the out of plane measurements. As a computationally inexpensive method to independently calculate local easy axis of the eight Dy ions, a point charge model also provides an estimate of the composition of the ground state wave function for each uncoupled Dy ion. The electrostatic calculations determine that the ground state wave-function of each Dy ion is $m_J = \pm15/2$ (>99%), in contrast
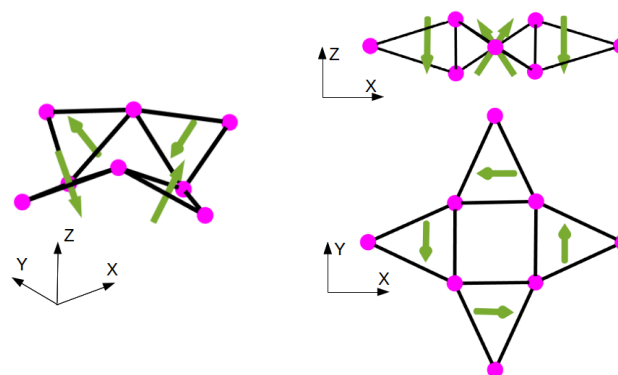
with magnetisation data which suggests significant mixing from excited Stark levels. Despite this limitation the point charge calculated local easy axis directions ($\phi_1 = 90\pm1°$, $\phi_2 = 90\pm1°$, $\theta_1 = 12\pm3°$ and $\theta_2 = 12\pm1°$) are found to be very similar with the values obtained fitting the experimental results to Eq. (1).

Discussion

Both experimental results and electrostatic calculations identify a Dy_8 ground state composed of four interlaced toroidal triangles. Each triangular unit have local easy axes lying approximately within the plane of the triangle. However as triangular units each share a side around a distorted tetrahedron, neighbouring triangles are pitched in opposing directions. The spin frustration in the central cubane of this system takes the form of a single-molecule spin ice analog. This allows exploring the effects of complex level crossing structure in a zero-dimensional object. Fig. 7 shows a schematic of the toroidal moments generated by each triangle within the Dy_8 ground state (green arrows). Neighbouring triangular units are canted anti-parallel resulting in a vortex antiferrotoroidic state. Perspectives within the plane reveals the pitching of toroic moments more clearly. The consequence is a doubly degenerate ground state of opposing antiferrotoroidic vortex chirality.

To better understand the applied field response of Dy_8 we have analysed the orientation dependence of single-crystal magnetisation with the effective Hamiltonian (Eq. 1) solution used to fit the experimental results. The calculated decomposition of equilibrium magnetisation as a function of field for each Dy ion reveals the microscopic spin structure within the Dy_8 molecule (Fig. 8). At fields less that c_1 the toroidal-vortex ground state is insensitive to applied field. At the first field crossing, c_1, a step in magnetisation is observed which corresponds with breaking of the vortex texture of the molecule. The field-induced ground state changes at c_1 and c_2 depend on in-plane molecule orientation. With an applied field along the molecular X or Y axis, c_1 is at the highest applied magnetic field and c_2 is at the lowest applied magnetic field with respect to other in-plane directions. The internal magnetisation microstates of this process are shown in Fig. 8a. At c_1, the outer spins (purple) align with the applied field in a process that
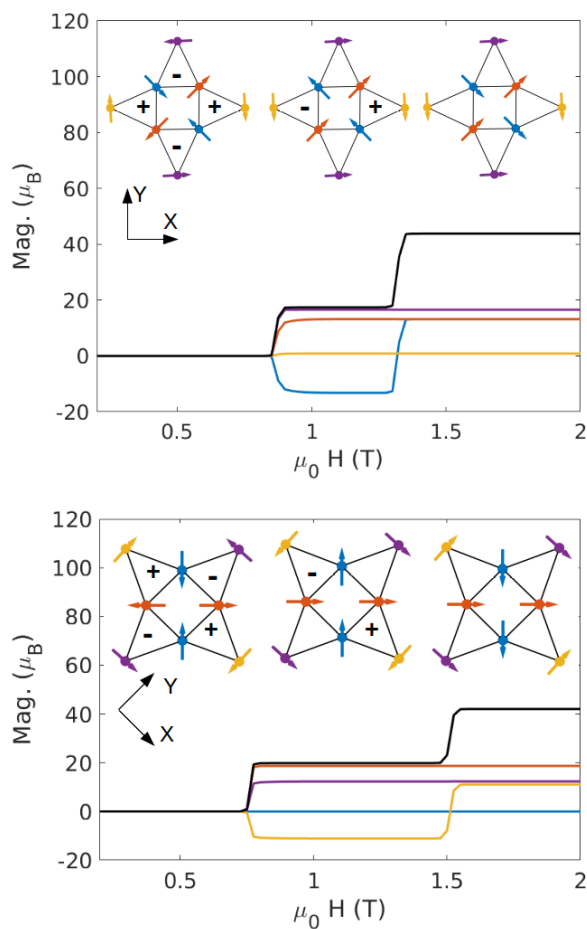
Fig. 8 Calculations of equilibrium magnetisation at 50 mK (black) with applied fields along X and at 45 degrees from X within the X-Y plane (adopting the same coordinate system from figure 7). The unique contributions to the molecular magnetisation curve from Dy ions are colour coded with respect to schematics (purple, yellow, red, and blue).

is coupled with toroidal switching from + to - for the left-most triangle; the local magnetisation of the right-most triangle remains unchanged, while the top and bottom triangles lose their toroidal configuration. At c_2, the remaining two central spins (blue) are reversed to align with the applied field and no toroidal moment in any of the four triangles persists. In a field applied at 45 degrees from the X or Y axis, c_1 is at the lowest applied magnetic field and c_2 is at the highest applied magnetic field with respect to other in-plane directions. Fig. 8b, shows how at c_1 the outer two purple spins align with the field direction and the top left triangle switches toroidicity. The second step in magnetisation at c_2 corresponds with the flipping of yellow spins parallel to applied field in a process that also involves flipping in the orientation of both blue spins. In summary the ground state of Dy_8 in zero field and applied fields up to c_1 is as a antiferrotoroidic tetramer, from c_1 to c_2 a antiferrotoroidic dimer and in fields greater than c_2 Dy_8 is non-toroidal. The canting of individual triangles within Dy_8 results in a canted antiferrotoroidic tetramer, giving rise to a toroid of toroids. Slowing of magnetic relaxation is observed on switching between antiferrotoroidic states. This is consistent with recent calculations that have indicated that ferrotoroidicity can compete with quantum tunnelling of magnetisation, slowing magnetic relaxation.[20]

Conclusions

The large cluster size, combined with non-colinear anisotropy and weak exchange coupling makes Dy_8 a considerably complex system to precisely evaluate magnetism. Consequently a multitude of approximations have to be applied at each level of analysis. Despite this we identify a Hamiltonian that precisely reproduces the magnetism of Dy_8, and remarkably the orientation of the single ion anisotropy axes obtained are consistent with simple electrostatic calculations. The simplified model provides insights into the internal structure of magnetisation for Dy_8 enabling conclusions regarding toroic states and comprehension of low energy excited states. Single-crystal magnetisation measurements reveal a combination of SMT and SMM characteristics; with both antiferrotoroidism in combination with slow magnetic relaxation and magnetic hysteresis. The ground state of Dy_8 is found to involve an antiferrotoroic tetramer. Low temperature measurements on a Dy_8 single-crystal reveal a two stepped magnetisation response in the molecular easy-plane that coincides with a step-wise deconstruction of antiferrotoroidism. These steps have a distinct in-plane angular dependence that is used to infer the easy axis orientations of the eight Dy ions. This study provides needed experimental evidence for SMT behaviour. It will be interesting to see how these results compare to *ab initio* calculations, and if such calculations can further improve the fit to the experimental results reported here. The utility of magnetisation measurements to extract single ion easy axes is inhibited in cases where the cluster symmetry follows closely the symmetry of the toroidal unit, including the archetype SMT Dy_3. This restriction is lifted when the cluster rotational symmetry axis is not collinear with the individual toroidal axes. This study highlights the potential of detailed single-crystal magnetisation measurements as an experimental probe that can support *ab initio* calculations in the identification and classification of SMTs.

From the standpoint of both high density information storage and quantum information processing, SMTs represent a promising avenue where coordination chemistry and nanoscale information processing could potentially intersect. The sensitivity of SMTs to electrical fields could enable the ultra-strong coupling regime required for the practical implementation of a scalable quantum computation architecture.[24] However before such applications can ever become a reality it is necessary to develop experiments that can explore the structure of eigenstates within prototype clusters. To date experimental investigations of SMTs and magnetoelectric coupling within molecular nanomagnets have been scarce [25,26], however molecules like Dy_8 represent promising candidates to expand such investigations.

Experimental and Theoretical Methods

Measurements

Magnetisation and susceptibility measurements down to 1.7 K were carried out on single-crystals and powder samples in a

Quantum Design MPMS SQUID magnetometer equipped with a 5.5T magnet. Angular dependent magnetisation measurements down to 0.25 K were performed on a single-crystal mounted on a micro-Hall sensor in a commercially made Oxford top-loading ^{3}He Cryostat (HelioxTL system) equipped with a 13T magnet. Single-crystals were encapsulated within a thin layer of fast setting epoxy resin to preserve them from drying out during magnetic measurements. The Dy$_8$ crystals have a plate like morphology that coincides with the best-mean-plane of the Dy$_8$ clusters within the unit cell. The two octanuclear clusters within the unit cell have parallel mean planes (Fig. 1(c)). The orientation of the two Dy$_8$ clusters are related by a 180° inversion, hence the coordinate system for single-crystal magnetism can be simplified to a molecular-based X-Y plane and Z axis as defined in Figure 7.

Calculations

Magnetisation simulations and Zeeman diagrams were calculated in *MATLAB* with use of the EasySpin[27]. Point charge calculations were performed using the SIMPRE computational package, version 1.1.[28] The calculations were performed for each Dy site using point charges to represent the other Dy ions (3+ charge), single bridging oxygen atoms (-1 charge), coordinated oxygen's (-0.5 charge) and the central μ_4 oxido (-2 charge). The positions of point charges were determined from crystallographic coordinates. The resultant crystal field splits the $J=15/2$ ground state, giving the uncoupled eigenvalues and wave-functions, including the orientation of the easy axis of the ground state Kramers doublet, for each uncoupled Dy site within the molecule. For each Dy site the ground state Kramers doublet was found to be close to pure $m_J = \pm|15/2\rangle$ with the first excited, $m_J = \pm|13/2\rangle$, doublet being more than 100 cm^{-1} higher in energy. Additional calculations were performed with another point charge calculation software, MAGELLAN[29]. We confirm that both SIMPRE and MAGELLAN results are equivalent.

Acknowledgments

References

1 C. A. P. Goodwin, F. Ortu, D. Reta, N. F. Chilton and D. P. Mills, *Nature*, 2017, **548**, 439–.

2 F.-S. Guo, B. M. Day, Y.-C. Chen, M.-L. Tong, A. Mansikkamäki and R. A. Layfield, *Science*, 2018, **362**, 1400–1403.

3 S.-D. Jiang, B.-W. Wang, G. Su, Z.-M. Wang and S. Gao, *Angewandte Chemie International Edition*, 2010, **49**, 7448–7451.

4 Y.-S. Ding, K.-X. Yu, D. Reta, F. Ortu, R. E. P. Winpenny, Y.-Z. Zheng and N. F. Chilton, *Nature Communications*, 2018, **9**, 3134–.

5 J. Luzon, K. Bernot, I. J. Hewitt, C. E. Anson, A. K. Powell and R. Sessoli, *Phys. Rev. Lett.*, 2008, **100**, 247205.

6 P.-H. Guo, J.-L. Liu, Z.-M. Zhang, L. Ungur, L. F. Chibotaru, J.-D. Leng, F.-S. Guo and M.-L. Tong, *Inorganic chemistry*, 2012, **51**, 1233–1235.

7 L. Ungur, S. K. Langley, T. N. Hooper, B. Moubaraki, E. K. Brechin, K. S. Murray and L. F. Chibotaru, *Journal of the American Chemical Society*, 2012, **134**, 18554–18557.

8 I. J. Hewitt, J. Tang, N. Madhu, C. E. Anson, Y. Lan, J. Luzon, M. Etienne, R. Sessoli and A. K. Powell, *Angewandte Chemie International Edition*, 2010, **49**, 6352–6356.

9 Y.-X. Wang, W. Shi, H. Li, Y. Song, L. Fang, Y. Lan, A. K. Powell, W. Wernsdorfer, L. Ungur, L. F. Chibotaru *et al.*, *Chemical Science*, 2012, **3**, 3366–3370.

10 S. Xue, X.-H. Chen, L. Zhao, Y.-N. Guo and J. Tang, *Inorganic chemistry*, 2012, **51**, 13264–13270.

11 G. Novitchi, G. Pilet, L. Ungur, V. V. Moshchalkov, W. Wernsdorfer, L. F. Chibotaru, D. Luneau and A. K. Powell, *Chemical Science*, 2012, **3**, 1169–1176.

12 S.-Y. Lin, W. Wernsdorfer, L. Ungur, A. K. Powell, Y.-N. Guo, J. Tang, L. Zhao, L. F. Chibotaru and H.-J. Zhang, *Angewandte Chemie*, 2012, **124**, 12939–12943.

13 M. Trif, F. Troiani, D. Stepanenko and D. Loss, *Phys. Rev. Lett.*, 2008, **101**, 217201.

14 A. Soncini and L. F. Chibotaru, *Phys. Rev. B*, 2010, **81**, 132403.

15 D. I. Plokhov, A. I. Popov and A. K. Zvezdin, *Phys. Rev. B*, 2011, **84**, 224436.

16 J. Tang, I. Hewitt, N. T. Madhu, G. Chastanet, W. Wernsdorfer, C. E. Anson, C. Benelli, R. Sessoli and A. K. Powell, *Angewandte Chemie International Edition*, 2006, **45**, 1729–1733.

17 A. Soncini and L. F. Chibotaru, *Phys. Rev. B*, 2008, **77**, 220406.

18 L. Chibotaru, L. Ungur and A. Soncini, *Angewandte Chemie*, 2008, **120**, 4194–4197.

19 G. Fernandez Garcia, D. Guettas, V. Montigaud, P. Larini, R. Sessoli, F. Totti, O. Cador, G. Pilet and B. Le Guennic, *Angewandte Chemie International Edition*, 2018, **0**, 17089.

20 K. R. Vignesh, A. Soncini, S. K. Langley, W. Wernsdorfer, K. S. Murray and G. Rajaraman, *Nature Communications*, 2017, **8**, 1023.

21 Z. Salman, S. R. Giblin, Y. Lan, A. K. Powell, R. Scheuermann, R. Tingle and R. Sessoli, *Phys. Rev. B*, 2010, **82**, 174427.

22 M. Gysler, F. El Hallak, L. Ungur, R. Marx, M. Hakl, P. Neugebauer, Y. Rechkemmer, Y. Lan, I. Sheikin, M. Orlita *et al.*, *Chemical Science*, 2016, **7**, 4347–4354.

23 D. I. Alexandropoulos, A. Fournet, L. Cunha-Silva, A. M. Mowson, V. Bekiari, G. Christou and T. C. Stamatatos, *Inorg. Chem.*, 2014, **53**, 5420–5422.

24 M. D. Jenkins, D. Zueco, O. Roubeau, G. Aromí, J. Majer and F. Luis, *Dalton Trans.*, 2016, **45**, 16682–16693.

25 A. K. Boudalis, J. Robert and P. Turek, *Chemistry Ű A European Journal*, 2018, **24**, 14896–14900.

26 J. Liu, J. Mrozek, W. K. Myers, G. A. Timco, R. E. P. Winpenny,

B. Kintzel, W. Plass and A. Ardavan, *Phys. Rev. Lett.*, 2019, **122**, 037202.

27 S. Stoll and A. Schweiger, *Journal of Magnetic Resonance*, 2006, **178**, 42 – 55.

28 J. J. Baldoví, S. Cardona-Serra, J. M. Clemente-Juan, E. Coronado, A. Gaita-Ariño and A. Palii, *Journal of Computational Chemistry*, 2013, **34**, 1961–1967.

29 N. F. Chilton, D. Collison, E. J. McInnes, R. E. Winpenny and A. Soncini, *Nat. Commun.*, 2013, **4**, 2551.
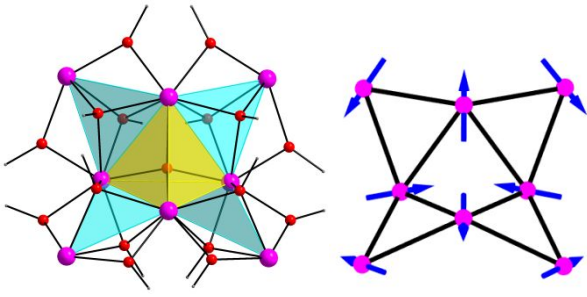
Multi-orientation single-crystal magnetisation measurements unpick the spin structure of Dy_8, identifying a canted antiferrotoroidic tetramer ground-state with slow magnetic relaxation.